89Zr-Labeled Multifunctional Liposomes Conjugate Chitosan for PET-Trackable Triple-Negative Breast Cancer Stem Cell Targeted Therapy

Rui Yang [1],*
Mudan Lu [2],*
Lan Ming [1],*
Yu Chen [1]
Kai Cheng [1]
Jie Zhou [1]
Shiwen Jiang [1]
Zhenyu Lin [3]
Daozhen Chen [1]

[1]Research Institute for Reproductive Health and Genetic Diseases, Affiliated Wuxi Maternity and Child Health Care Hospital of Nanjing Medical University, Wuxi 214002, People's Republic of China; [2]Internal Medicine, Affiliated Wuxi Maternity and Child Health Care Hospital of Nanjing Medical University, Wuxi 214002, People's Republic of China; [3]Ministry of Education Key Laboratory for Analytical Science of Food Safety and Biology, Fujian Provincial Key Laboratory of Analysis and Detection for Food Safety, College of Chemistry, Fuzhou University, Fuzhou 350116, People's Republic of China

*These authors contributed equally to this work

Correspondence: Daozhen Chen
Research Institute for Reproductive Health and Genetic Diseases, Affiliated Wuxi Maternity and Child Health Care Hospital of Nanjing Medical University, Wuxi 214002, People's Republic of China
Tel +86-13584189188
Fax +86-510-82725094
Email chendaozhen@163.com

Purpose: Therapy for triple-negative breast cancer (TNBC) is a global problem due to lack of specific targets for treatment selection. Cancer stem cells (CSCs) are responsible for tumor formation and recurrence but also offer a promising target for TNBC-targeted therapy. Here, zirconium-89 (^{89}Zr)-labelled multifunctional liposomes (MLPs) surface-decorated with chitosan (CS) were fabricated to specifically target and trace cluster of differentiation 44^{+} (CD44^{+}) TNBC CSCs specifically.

Patients and Methods: The biological basis of CS targeting CD44 for cancer therapy was investigated by detecting the expression of CD44 in TNBC CSCs and TNBC tissues. Molecular docking and dynamics simulations were performed to investigate the molecular basis of CS targeting CD44 for cancer therapy. Gambogic acid (GA)-loaded, ^{89}Zr@CS-MLPs (^{89}Zr-CS-GA-MLPs) were prepared, and their uptake and biodistribution were observed. The anti-tumor efficacy of ^{89}Zr@CS-GA-MLPs was investigated in vivo.

Results: CD44 is overexpressed in TNBC CSCs and tissues. Molecular docking and dynamics simulations showed that CS could be stably docked into the active site of CD44 in a reasonable conformation. Furthermore, ^{89}Zr@CS-GA-MLPs were able to bind specifically to CD44^{+} TNBC stem-like cells and accumulated in tumors of xenograft-bearing mice with excellent radiochemical stability. ^{89}Zr@CS-GA-MLPs loaded with GA showed remarkable anti-tumor efficacy in vivo.

Conclusion: The GA-loaded, ^{89}Zr-labelled, CS-decorated MLPs developed in this study represent a novel strategy for TNBC imaging and therapy.

Keywords: radionuclide, PET, CS, CD44, molecular docking, molecular dynamics simulation

Introduction

Breast cancer is still the most common cancer in women worldwide, with approximately 0.5 million people dying from it in 2015.[1] Due to increases in public awareness of cancer prevention, as well as improved levels of diagnosis and treatment, there have been modest improvements in breast cancer outcomes.[1,2] However, breast cancer is a highly heterogeneous disease. Triple-negative breast cancer (TNBC), which accounts for about 20% of cases, is generally more aggressive, with higher rates of recurrence and metastases, and a lack of effective therapeutic targets.[3] Patients with TNBC of all subtypes have the worst prognosis,

which greatly affects the overall prognosis of breast cancer. Although considerable effort has been put into discovering new therapeutic approaches, progress is slow and there have been few substantive breakthroughs.

Cancer stem cell (CSC) theory states that CSCs are a small population of cells within cancers, with unlimited proliferative capacity that inevitably drive tumor recurrence and metastasis after therapy.[4] Traditional treatments often focus on shrinking the bulk of tumors or decreasing the number of tumor cells; however, tumors tend to recur after a certain period of time, resulting in residual CSCs and resistance to treatment.[5] As a consequence, CSCs present an obstacle to cancer therapy while also providing therapeutic targets on tumors in cases like TNBC. Breast cancer provided the first solid tumors that demonstrated the existence of CSCs, and the cluster of differentiation (CD) $44^+CD24^{-/(low)}$ phenotype has become one of the most typical breast CSC surface makers.[6] Compared with non-TNBC cases, the proportion of $CD44^+CD24^{-/(low)}$ cells seems to be higher in TNBC cases.[7] In addition, studies have demonstrated that high expression of CD44 was correlated with a lack of estrogen receptor (ER), progesterone receptor, and epidermal growth factor receptor (HER2) expression; the $CD44^+CD24^-$ phenotype is also predictive of a poor prognosis.[8] Using immunofluorescence (IFC) staining, the present study found high expression of CD44 in breast cancer tissues from 32 female patients. The design of CD44-targeted therapeutic modalities will be critical for the treatment of TNBC, given the growing body of evidence indicating that TNBC CSCs overexpress CD44 receptors.

CD44 is a transmembrane glycoprotein that is widely distributed on the surface of many normal cells[9] and a variety of solid tumor cells.[10] Therefore, specificity should be considered first in any strategy for CD44 target therapy. A recent study showed that nanoparticles decorated with the biocompatible and biodegradable natural polysaccharide chitosan (CS) could target $CD44^+$ CSCs while reducing drug accumulation in normal $CD44^+$ stem cells.[11] The author suggested that the partial structural similarity of CS to the CD44 ligand hyaluronic acid (HA) and its positive charge contributed to a more efficient bond between the nanoparticle and $CD44^+$ CSCs. However, the exact binding mechanism, especially at the molecular level, remains unclear. Here, for the first time, we used molecular docking and dynamics simulations to reveal the binding mechanism and found that CS can dock into the active site of CD44 in

a reasonable conformation. The distribution of CD44 expression was detected by IFC staining in TNBC patients. The $CD44^+$ CSCs were enriched using a 3D mammosphere enrichment method, as reported previously.[12] Based on this, a CS-decorated, multifunctional liposome system was designed and prepared to target $CD44^+$ CSCs in vitro and in vivo. Furthermore, the liposome surface was labeled with zirconium-89 (^{89}Zr), and positron emission tomography (PET) imaging was used to trace the CS-decorated, multifunctional targeted system's behavior accurately and quantitatively in vivo and in real time. What is more, gambogic acid (GA) was loaded in the MLPs to investigate the antitumor effect of multifunctional targeted system in vivo (Scheme 1).

Patients and Methods
Patients and Tissue Specimens
The study included a total of 32 female patients who were diagnosed with TNBC by histopathological analysis between Aug. 2017 and Jun. 2019 at the Affiliated Wuxi Maternity and Child Health Care Hospital of Nanjing Medical University (Wuxi, China). Patients were between 34 and 73 years of age (median age, 52 years). Patients who had previously undergone radiotherapy, chemotherapy, or other treatment prior to surgery were excluded from this study. Histological specimens were collected, fixed with formalin, and embedded in paraffin for histopathological diagnosis and IFC staining after surgery. All patients provided informed consent and the current study was approved by the Ethics Committee of Nanjing Medical University (No. (2016) 276). It was also performed in accordance with the Code of Ethics of the World Medical Association, with the ethical standards of the responsible committee on human experimentation (institutional and national), and with the Helsinki Declaration of 1975, as revised in 2000.

IFC Staining
Anti-CD44 mouse antibody was used for CD44 IFC staining. Antigen retrieval was performed using EDTA microwave methods. Following primary antibody binding, the slides were incubated with MultiVision Polymer Cocktail. The nucleus was re-dyed with DAPI. The expression of CD44 on cells was visualized and photographed using a fluorescence microscope. Cells stained with red in the membranous were regarded as positive for CD44.
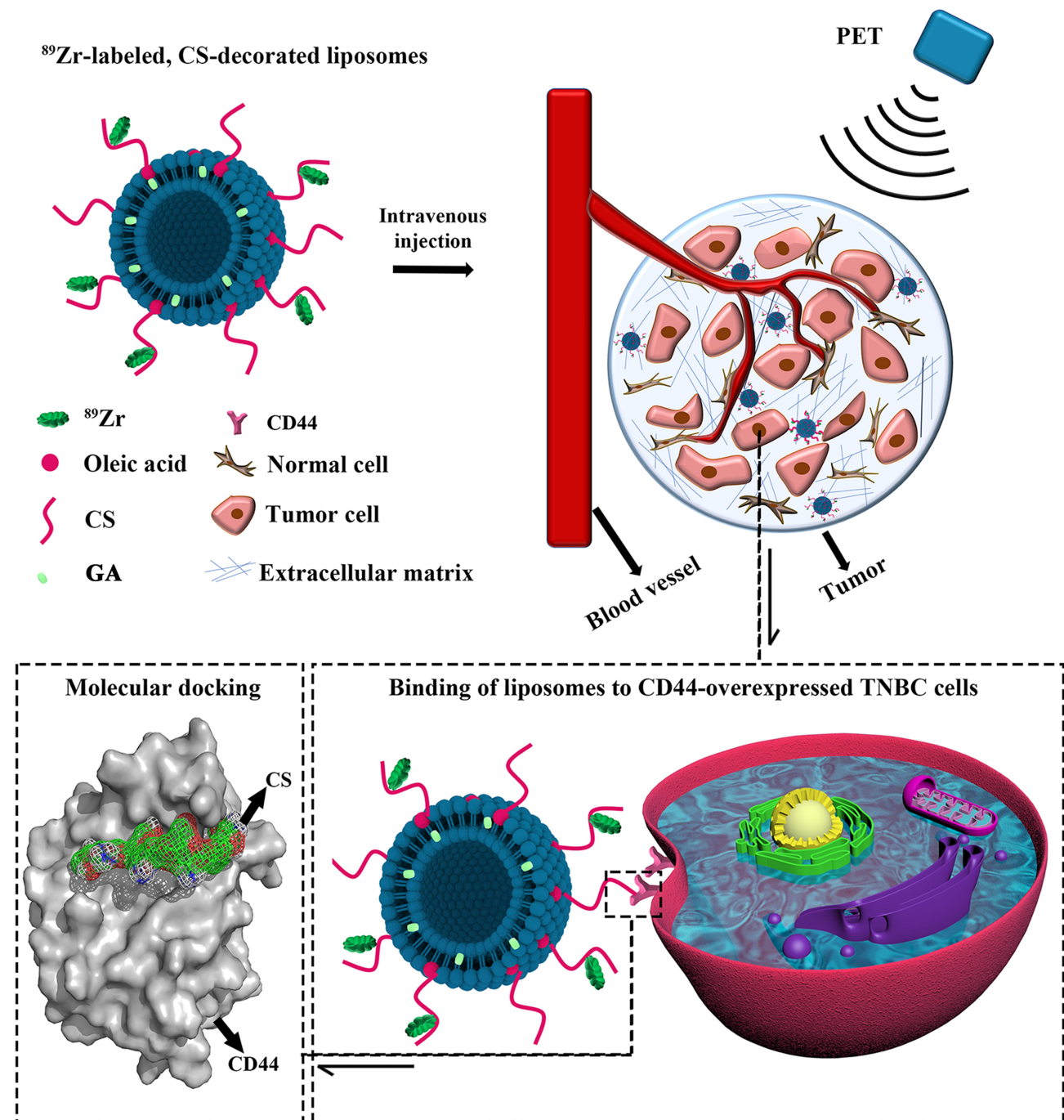
Scheme I Scheme of formation, and accumulation of [89]Zr-labeled, GA-loaded, CS-decorated liposomes as a multifunctional targeted therapy system. PET imaging was used to trace the biodistribution of liposomes. The binding mechanism was analyzed by molecular docking.
Abbreviations: CS, chitosan; PET, positron emission tomography; CD, cluster of differentiation; TNBC, triple-negative breast cancer; GA, gambogic acid; [89]Zr, zirconium-89.

3D Mammosphere Culture from MDA-MB-231 Cells

MDA-MB-231 cells were obtained from the Institute of Biochemistry and Cell Biology. The 3D mammospheres of MDA-MB-231 cells were cultured using DMEM/F_{12} (1:1) supplemented with 20 μg/L recombinant human epidermal growth factor (hEGF), 20 μg/L basic fibroblast growth factor, and 2% B27 in a low-adhesion culture bottle at 1×10^5 single cells/mL. Cells placed in a 10% serum environment and adhesion culture (called a 2D culture) were used as a control group. After 7 days, the morphology of the 3D mammospheres was observed.

Flow Cytometry

After 7 days, the 3D mammospheres were collected and incubated with PE-conjugated anti-CD44 monoclonal antibody and APC-conjugated anti-CD24 monoclonal antibody at 4°C for 30 min and then analyzed by flow cytometer.

Molecular Docking

The three-dimensional structure of human CD44 protein was obtained from RCSB Protein Data Bank (www.rcsb.org, pdb ID: 2JCQ). The docking was prepared after minimizing the energy of the CS (n = 2) structure (ChemiBiodraw 14.0). Conformational docking was performed about 100 times using the Autodock 4.0 program. The binding site and energy were analyzed by choosing the conformation with lowest docking energy. The results were visualized using PyMOL.

Molecular Dynamics Simulations

The GROMACS 2018 software package was used to perform molecular dynamics simulations. Water molecules were simulated using the extended simple point charge model (SPC/E) model. The complex system was placed in the center of a cube with a size of $7 \times 7 \times 7$ nm and the distance between each atom of the protein and the box was greater than 1.0 nm. The box was randomly filled with water molecules, which were replaced with 4 NA^+ ions to make the simulated system electrically neutral. A two-step MD simulation method was used to optimize the interaction between the target protein and the solvent and ions. Steepest descent energy minimization was performed to optimize the system by keeping it at the lowest energy state. This was followed by a restricted MD simulation to balance the system for canonical ensemble and isothermal-isobaric ensemble. Newtonian motion equations were calculated using the Verlet algorithm with a time step of 2 fs. The Van der Waals force was calculated using the Lennard-Jones potential with a non-cutoff distance fixed at 1.2 nm. Bond length of all atoms was constrained using the LINCS algorithm. The particle mesh Ewald (PME) was used to calculate long-range electrostatic interactions with a grid width of 0.16 nm. The systems were run at conditions of periodic boundary and constant pressure and temperature. Temperature and pressure were fixed at 310 K and 1 bar, respectively, using V-rescale 22 with a relaxation time of 0.1 ps for temperature and the Parrinello–Rahman method for pressure coupling with a relaxation time of 0.5 ps. The molecular dynamics simulation was conducted for 100 ns.

Synthesis of CS-Decorated MLPs (CS-MLPs) and Radiolabeling with [89]Zr

The CS-MLPs were prepared using previously reported methods with slight modification. First, 65 mg 1-(3-dimethylaminopropyl)-3-ethylcarbodiimide hydrochloride (EDC), 39 mg of N-Hydroxysuccinimide (NHS), and 0.3 mL oleic acid were added to 80 mL methanol. The mixture was then added dropwise to 100 mL CS solution (0.01 mg/mL) in acetic acid (1%), followed by stirring for 48 h at room temperature. The reaction mixture was precipitated with $NH_3 \cdot H_2O$, and the precipitation was further washed with methanol and purified by dialysis against distilled water (molecular weight cutoff, MWCO 1000, 4×2 L). Finally, the oleic acid–CS solution was lyophilized and stored at −20°C for later use. The CS-MLPs were prepared using the thin-film dispersion method. Briefly, the lecithin, cholesterol, and oleic acid–CS were dissolved in 10 mL of a chloroform and methanol mixture (v/v, 3:2) at a mass ratio of 10:1:1. The mixture was placed on a rotary evaporator for 30 min at 90 rpm to remove the chloroform and methanol. The resulting film was hydrated in 10 mL phosphate buffer saline (PBS, pH 7.2) in a water bath for 1 h at room temperature. To obtain the CS-MLPs with uniform particle size, the mixture was treated with an ultrasound probe for 5 min with an amplitude of 30% and an interval of 3 s.

To detect the uptake and distribution of the nanomaterials in 3D mammospheres in vitro, CS-MLPs with rhodamine (Rh)-B-loaded materials (CS-Rh-MLPs) were prepared using the thin-film dispersion method. Briefly, lecithin, cholesterol, Rh, and oleic acid-CS were dissolved in 10 mL of a chloroform and methanol mixture (v/v, 3:2) at a mass ratio of 10:1:1:1. The mixture was placed on a rotary evaporator for 30 min at 90 rpm to remove the chloroform and methanol. The resulting film was hydrated in 10 mL PBS (pH 7.2) in a water bath for 1 h at room temperature. To obtain the CS-Rh-MLPs with uniform particle size, the mixture was treated with an ultrasound probe for 5 min, using an amplitude of 30% and an interval of 3 s. Finally, the non-encapsulated Rh was removed by centrifugation at 6000 rpm for 10 min, 3 times.

To detect the uptake, distribution and anti-tumor effect of the nanomaterials in vivo, [89]Zr@CS-GA-MLPs were prepared. Briefly, 300 μL oleic acid-CS was mixed with 600 μL 1 M $NaHCO_3$ solution, and adjusted to pH 9 by adding 1 M Na_2CO_3. Then, 0.1 mg deferoxamine (DFO) was added to the above solution and allowed to react for 2 h at 37°C, and shake once every 10 min. After the

reaction was completed, the solution was centrifuged and purified by ultrafiltration centrifuge tube (4000 rpm for 5 min) and washed with 0.15 M acetate buffer solution 3 times to obtain the DFO modified oleic acid–CS (DFO-CS). After freeze drying, lecithin, cholesterol, GA, DFO-CS and oleic acid-CS were dissolved in 10 mL of a chloroform and methanol mixture (v/v, 4:1) at a mass ratio of 20:2:2:1:1. The rotary evaporation-hydration step was performed as previously for preparation of CS-Rh-MLPs. Then, 40 μL ^{89}Zr oxalic acid solution (1 mCi) was mixed with 0.5 mL HEPES solution, and adjusted to pH 7 by adding 20 μL 1 M NaHCO$_3$ solution. Then, 500 μL CS-GA-MLPs were added to the system and reacts for 60 min at 37°C. After the reaction was completed, the solution was centrifuged and purified through ultrafiltration centrifuge tube (4000 rpm for 5 min), and washed with 0.15 M acetate buffer solution for 3 times to obtain the ^{89}Zr@CS-GA-MLPs.

Characterization of CS-MLPs

Transmission electron microscopy (TEM, Hitachi, Tokyo, Japan) was used to determine the morphology and structure of CS-MLPs. The size was evaluated by ZetaPlus analysis (Brookhaven Instruments Co., Holtsville, NY, USA). Storage stability of CS-MLPs was observed at 4°C for 3 weeks.

Uptake of CS-Rh-MLPs in 3D Mammospheres

Confocal laser scanning microscopy was used to assess the uptake and distribution of CS-Rh-MLPs in 3D mammospheres, which were incubated with CS-Rh-MLPs (target group) for 1 h at 37°C in 5% CO$_2$. 3D mammospheres blocked with HA (pre-blocking group) were used as controls.

Animal Model

All animal experiments were conducted with the approval of the Animal Ethics Committee of Nanjing Medical University prior to the commencement of the study and in accordance with the Guidelines for the Care and Use of Experimental Animals established by the Ministry of Science and Technology of the People's Republic of China. Nude mice (female, aged 5 weeks) were obtained from the Comparative Medicine Centre of Yangzhou University (Jiangsu, People's Republic of China). The tumor model was established by subcutaneous injection of 1×10^6 MDA-MB-231 cells suspended in 100 μL PBS solution into the left flank of nude mice.

Biodistribution and Anti-Tumor Application of ^{89}Zr@CS-MLPs in vivo

Radioactive instant thin-layer chromatography was used to determine the radiochemical purity of the labeled product, ^{89}Zr@CS-GA-MLPs. The support consisted of silica gel-impregnated glass fiber sheets (Pall Corp., East Hills, NY), and citrate buffer (0.02 M, pH 5.0) was used as the developing agent. ^{89}Zr@CS-GA-MLPs were point on the sample line which was 1cm from the bottom of the chromatography strip. When the unfolding front reached 7cm, the chromatographic strip was removed, dried, and scanned using a Bioscan scanner, with a scanning distance of 8 cm. As free ^{89}Zr can form a ^{89}Zr-citric acid complex in citrate buffer, it is expected to be expanded (retention factor (Rf) = 0.7–0.9), whereas the labeled product, ^{89}Zr@CS-GA-MLPs would remain at the origin (Rf = 0.1–0.2) because of its high molecular weight.

Micro PET was used to determine the biodistribution of ^{89}Zr@CS-GA-MLPs in vivo. Nude mice bearing subcutaneously implanted human xenografts of MDA-MB-231 cells were injected with ^{89}Zr@CS-GA-MLPs via the tail vein and evaluated by Micro PET at 4, 8, 24, 48 and 96h after injection. The scanned data were iterated and reconstructed using the 3D ordered subset expectation maximization method (layer thickness 0.5 mm, matrix 280×280, energy window 350–650 keV). PMOD software was used to analyze the reconstructed data. Accumulation of radioactive (%injected dose per gram of tissue, %ID/g) in the regions of interest (ROI) in the tumor, heart, liver, kidney, lung and other tissues was calculated. The mice were treated with ^{89}Zr@CS-GA-MLPs once every other day. After 28 days, mice were sacrificed, and the organs, including the heart, liver, spleen, lung, and kidney were collected for hematoxylin and eosin (HE) staining.

The nude mice bearing subcutaneously implanted human xenografts of MDA-MB-231 cells were treated with PBS (control group), GA-MLPs (non-target group), and ^{89}Zr@CS-GA-MLPs (target group) once every other day. The mice bearing MDA-MB-231 tumors were injected intravenously with GA-MLPs or ^{89}Zr@CS-GA-MLPs (GA, 2 mg/kg). The tumor size was measured, and the volume was calculated according to the formula V = (a × b^2)/2, where a and b are the longest and widest diameters of the tumor, respectively. The change in body weight was plotted to determine the

tolerable safety profile. After 28 days of treatment, mice were sacrificed, and the tumors were collected for HE staining.

Statistical Analysis

Values are presented as means ± standard deviation. The data were analyzed using SPSS for Windows software (SPSS Inc., Chicago, IL). In all analyses, $p<0.05$ was taken to indicate statistical significance.

Results and Discussion
Biological Basis of CS Targeting CD44 for Cancer Therapy: Overexpression of CD44 in TNBC CSCs and TNBC Tissues

Ever since the CD44^{+}CD24^{−/low} breast CSCs were first isolated and identified from breast cancer patients by Al-Hajj,[6] CD44, either alone or in combination with other markers such as CD133 and CD24, has been considered a typical surface marker of breast CSCs. It is believed that CSCs have the ability to overcome anoikis and form spherical structures when cultures are suspended in serum-free medium. In our study, the 3D mammosphere culture method was used to enrich the TNBC CSCs as previously reported.[13] The TNBC cell line MDA-MB-231 can form a spherical structure after being cultured for 7 days (Figure 1A). The percentage of breast CSC marker CD44^{+}CD24^{−/low} in the 3D mammosphere was analyzed by FACS. The percentage of CD44^{+}CD24^{−/low} in 3D mammosphere was significantly higher than that in 2D culture cells (92.5% ± 4.4% vs 72.4% ± 5.6%, respectively, $p < 0.05$), which showed that 3D microsphere culture can enrich TNBC CSCs, and the TNBC CSCs overexpressed CD44 (Figure 1B).

As a subtype of breast cancer, TNBC lacks human epidermal growth factor receptor 2 (HER2) targets and expresses less than 1% of estrogens and progestogens.[14] As a result, endocrine therapy and anti-HER2 therapy are not suitable for TNBC, which leads to a higher risk of metastasis and lower overall survival rates compared with other molecular subtypes.[15] However, the overexpressed CD44 on the surface of TNBC tumor cells provides an ideal target for TNBC therapy. In our study, the expression of CD44 was successfully determined in all cases by IFC staining. As shown in Figure 1C, CD44 appeared red in the membranous staining and overexpressed in the tissues of all cases. Hence, the overexpression of CD44 in CSCs and TNBC tissues provides a promising approach with the potential to eliminate TNBC.

CSCs are a subpopulation of cells thought to have the ability to promote tumor infiltration and unlimited proliferation, and contribute to poor survival and prognosis.[4] CSCs also exist in breast cancer, and the CD44^{+}/CD24^{−} subpopulation is involved in the formation and promotion of tumor progression.[6] Studies have shown that the percentage of CD44^{+} CSCs in the TNBC cell line was higher than that in non-TNBC cell lines.[12] In addition, Zheng observed 139 breast invasive ductal carcinomas and found that the proportion of CD44^{+}CD24^{−} cases, CD44^{+} cases in the TNBC group were higher than that in the non-TNBC group.[7] This indicates that CD44 could be an ideal target for TNBC therapy. Furthermore, the role of CD44 in regulating cancer stemness, progression, and prognosis suggests that CD44 is a promising approach for eliminating CSCs and TNBC.

Molecular Basis of CS Targeting CD44 for Cancer Therapy: Molecular Docking and Molecular Dynamics Simulations

Common cancer treatment mainly includes radiotherapy, chemotherapy, surgery, or combined therapy. These therapies always reduce the number of tumor cells or tumor volume but cannot eradicate CSCs, which may lead to a treatment failure. Targeted nanoparticles that deliver one or more therapeutic agents to CSCs in tumor tissues might be an ideal approach for overcoming these issues.[16] Therefore, the selection of molecules conjugated onto the nanoparticles to target CD44^{+} cells is crucial for maximizing anti-tumor efficacy and minimizing the systemic side effects of the targeted nanoparticles. In addition, the existence of CD44 on many normal cells should also be considered. A previous study developed a CS-based strategy to target CD44 receptors overexpressed on non-TNBC CSCs but not expressed on normal stem cells; CS-decorated nanoparticles were able to destroy orthotopic xenografts of non-TNBC in mice with nearly no systemic side effects.[11] CS has unique features of biocompatibility and biodegradability, and its chemical structure partially resembles that of HA, a ligand of CD44.[17] In addition, CS has a positive charge, and therefore binds easily to mammalian cells, including CSCs.[18] In our study, we developed a CS-based strategy to target CD44^{+} TNBC CSCs and elucidated the binding mechanism at the molecular level.

Molecular Docking

To test the hypothesis that CS can target and bind to CD44 (Figure 2A), we used molecular docking to analyze the binding site and binding energy. CS was able to target and
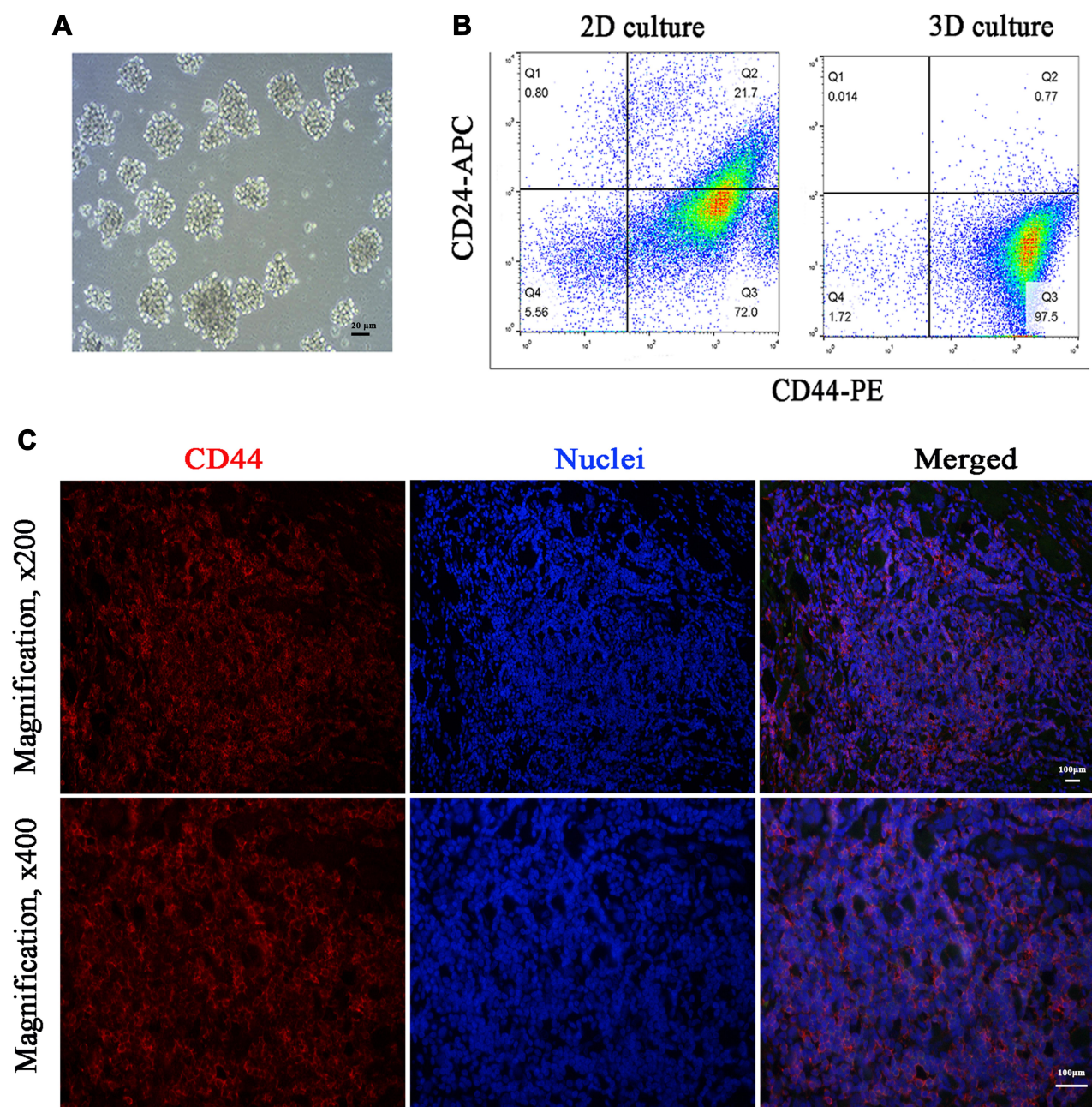
A

B

2D culture   3D culture

CD24-APC

CD44-PE

C

CD44   Nuclei   Merged

Magnification, x200

Magnification, x400

Figure 1 CD44 overexpression in TNBC CSCs and tissues. (**A**) 3D mammosphere after 7 days of culture (magnification, ×400). (**B**) CD44+ CSCs in TNBC 3D mammospheres. (**C**) CD44 staining in TNBC tissues. The red fluorescence of CD44 was observed on the membranes of most of the tumor cells (excitation 465–495 nm, emission 590 nm). The cell nuclei were visualized as blue fluorescence (excitation 330–380 nm, emission 420 nm).
Abbreviations: CD, cluster of differentiation; TNBC, triple-negative breast cancer; CSC, cancer stem cell; PE, p-phycoerythrin; APC, allophycocyanin.

bind to the active site of CD44 protein in a reasonable conformation through hydrophobicity and van der Waals force (Figure 2B). The docking required thirteen amino acids (GLU41, TYR46, GLU79, THR80, CYS81, ARG82, TYR83, ARG94, HIS96, ASN98, ILE100, CYS101, ASP120), and four hydrogen bonds were formed, including GLU41 (2.6 Å), GLU79 (2.4 Å), ASN98 (2.8 Å), ILE100 (2.5 Å) (Figure 2C and D).

Molecular Dynamics Simulations

To obtain more detailed information on the interaction between CD44 and CS, molecular dynamics simulations were used to evaluate the complex system. As shown in Figure 3A, following a 100 ns simulation, the Cα skeleton of the CD44-CS complex approached equilibrium after 20 ns, indicating that the conformation of the protein complex became stable, gradually, after 20 ns. The root-mean-square
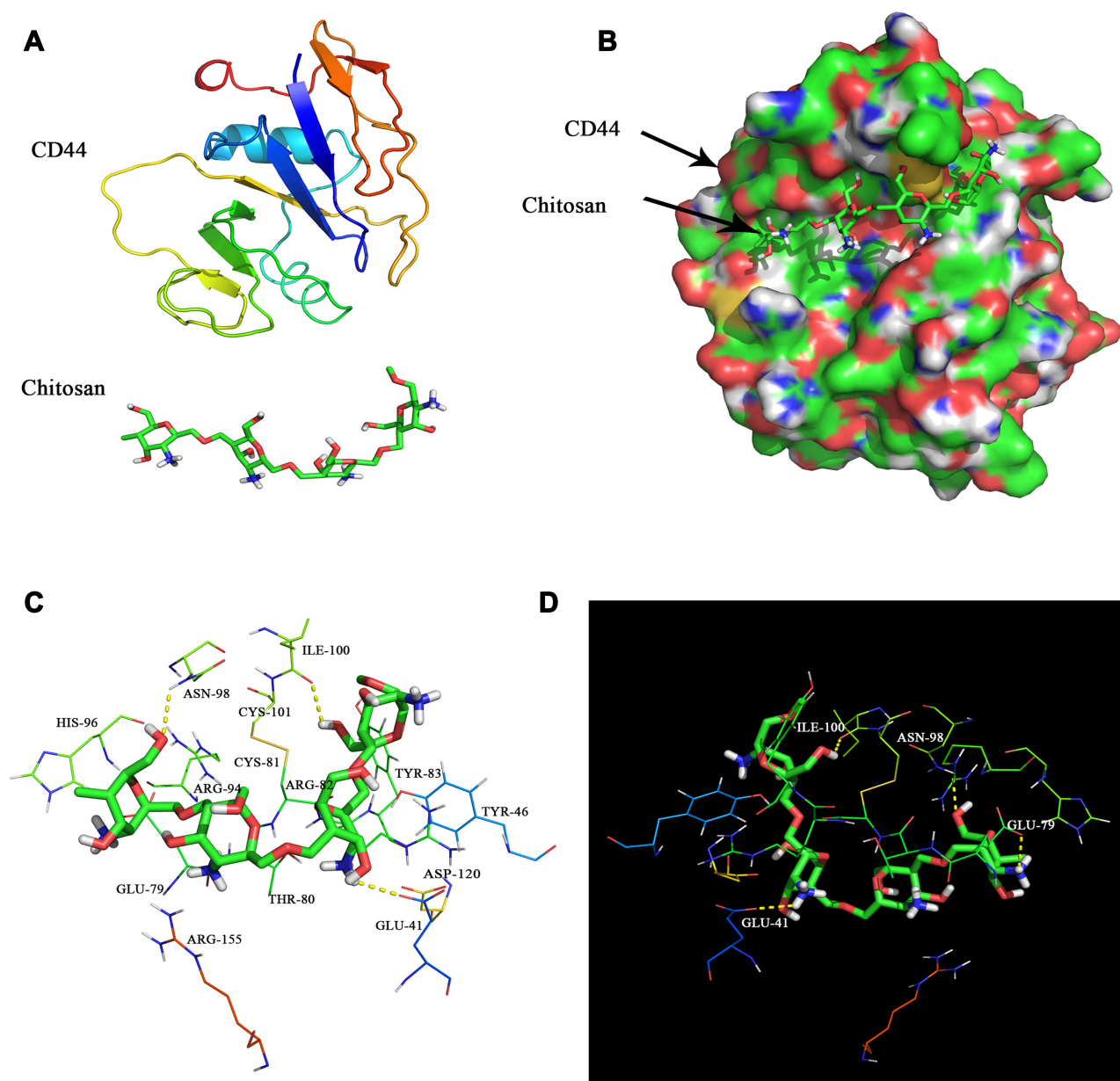
Figure 2 Molecular docking of CD44 and CS. (**A**) Chemical structures of CD44 and CS. (**B**) Schema of CS binding to CD44 protein. (**C**) The amino acid sequence of CD44 that interacts with CS. (**D**) CD44 interaction with CS via hydrogen bonding.
Abbreviations: CS, chitosan; CD, cluster of differentiation; HIS, histidine; ASN, asparagine; CYS, cysteine; ILE, isoleucine; ARG, arginine; TYR, tyrosine; GLU, glutamic acid; THR, threonine; ASP, aspartic acid.

deviations (RMSDs) of the Cα complex ranged from 0.1 to 0.3 nm, indicating that the conformation of the CD44-CS complex was stable. The root-mean-square fluctuations (RMSFs) of CD44 (amino acids 25–173) are shown in Figure 3B. In addition to the loop structure of the protein, amino acid regions 40–60 and 100–120 are more volatile than other regions. Therefore, it is speculated that the amino acids in this region represent an important functional region. The radius of gyration (Rg) value of CD44-CS was relatively stable and gradually recovered after a decrease during

molecular dynamics, which suggested that the whole structure of CD44 is tight at the beginning and rises up late during the process of CD44 binding to CS (Figure 3C). The total binding free energy was −442.306 kJ/mol. Electrostatic interaction is the main force in the binding free energy, followed by Van der Waals force, which explained, thermodynamically, how CS could target CD44 protein (Table 1). For the first time, we used molecular docking and dynamics methods to gain detailed insights into the binding process and mechanisms between CD44 and CS.
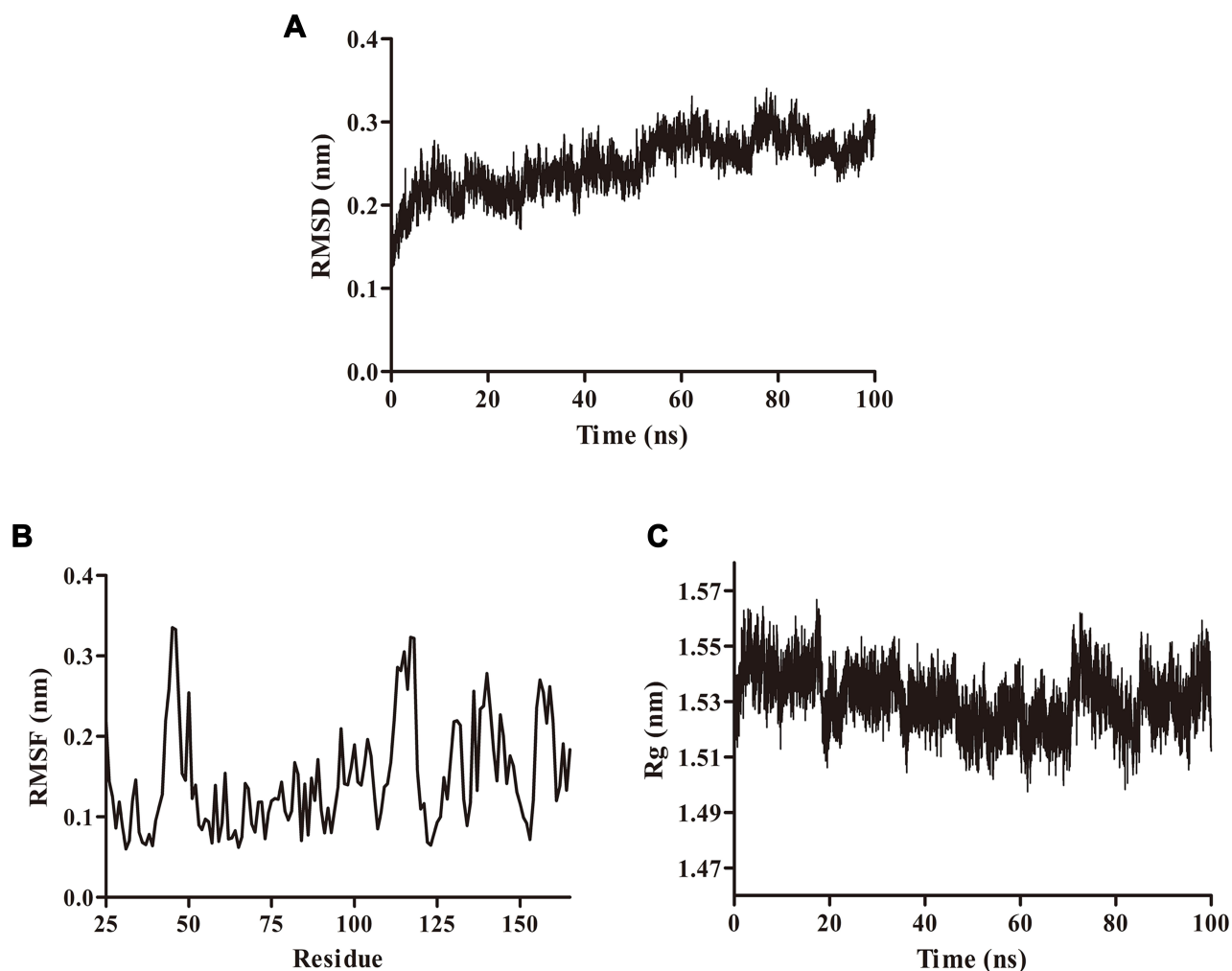
Figure 3 Molecular dynamics simulations. (**A**) The RMSD of the simulation calculated over 100 ns. (**B**) The RMSF of the simulation calculated over 100 ns. (**C**) The Rg of the simulation calculated over 100 ns.
Abbreviations: RMSD, root-mean-square deviation; RMSF, root-mean-square fluctuation; Rg, radius of gyration.

Synthesis of CD44-Decorated Liposomes for TNBC CSCs-Targeted Therapy

Characterization of CS-MLPs

At the beginning of our study, we found that CD44 was highly abundant in TNBC CSCs and tissues, and CS can effectively target and bind to CD44. For the first time, the binding process and mechanisms between CD44 and CS have been revealed by molecular docking and dynamics methods. Accordingly, CS-based liposomes (CS-MLPs) targeting CD44$^+$ TNBC CSCs were developed. Spherical blank liposomes and CS-MLPs were observed with diameters of 127.3 ± 0.8 nm and 158.4 ± 3.3 nm, respectively (Figure 4AD). This size means that MLPs can enter the tumor via enhanced permeability and retention (EPR) effects and bind to the tumor cells more easily.[19] Liposome stability is an important consideration before establishing a new, efficient drug-loaded nano-system.

Changes in particle size over time are considered a useful evaluation index of the stability of liposomal suspensions.[20] Therefore, to assess the stability of the CS-MLPs, the hydrodynamic size was determined in PBS, which showed no noticeable change over 3 weeks at 4°C, suggesting good stability (Figure 4E).

Binding of CS-MLPs to CD44-Overexpressed Cells in vitro and the Distribution and Anti-Tumor Effect in vivo

Rh-loaded CS-MLPs were prepared to determine the binding capacity in CD44-overexpressed 3D mammospheres through confocal laser scanning microscopy. A pre-blocking group (3D mammospheres blocked with HA) was used as a control. As expected, the cell membranes of 3D mammospheres exhibited red fluorescence in the

Table 1 Binding Free Energy Between CS and CD44

Force	Energy (kJ/mol)
Van der Waals force	−174.065
Electrostatic force	−485.916
Polar solvation free energy	238.583
Non-polar solvation free energy	−20.908
Total free energy	−442.306

Abbreviations: CS, chitosan; CD, cluster of differentiation.

target group at 1 h, and the fluorescence intensity was stronger than that of the pre-blocking group (Figure 5A). This suggests that CS-MLPs can bind to CD44-overexpressed cells and might be a good carrier to deliver the therapeutic drug to TNBC tissues.

To investigate further the biodistribution of CS-MLPs, they were conjugated with DFO via the amine groups of CS on the surface of [89]Zr@CS-GA-MLPs. The [89]Zr-labeling efficiency of [89]Zr@CS-GA-MLPs was measured using HPLC. [89]Zr@CS- GA-MLPs were obtained with a 50% labeling efficiency and >95% radiochemical purity. The biodistribution and targeting ability of [89]Zr@CS- GA-MLPs were observed in the nude mice bearing subcutaneously implanted human xenografts of MDA-MB-231 cells after intravenous injection. PET imaging was obtained at four different time points. As shown in Figure 5B and Table 2, [89]Zr@CS- GA-MLPs were accumulated mainly in tumors ($7.04 \pm 1.00\%ID/g$) within 96 h post-injection (p.i.) at significantly higher levels than those in the heart ($5.37 \pm 0.48\%ID/g$), spleen ($4.7 \pm 1.23\%ID/g$), kidney ($2.57 \pm 1.16\%ID/g$), and lung ($1.69 \pm 0.58\%ID/g$). ROI analysis of the tumor showed that radioactivity accumulation of 3.46 ± 0.33, 4.13 ± 0.24, 6.61 ± 0.30, 7.52 ± 0.43, $7.04 \pm 1.00\%ID/g$ at 4, 8, 24, 48 and 96 h p.i., respectively (n = 3). Although the half-life of [89]Zr is about 70 h, MLPs accumulation in tumors at 48 and 96 h showed no obvious difference (p>0.05). The observation is probably due to the fact that the [89]Zr@CS-GA-MLPs have long circulation characteristics so to enhance uptake of tumor. The PET signal in liver is higher than that in the tumor at different times, it probably due to liver is not only a major blood poor of the body but also major site of liposome metabolism in vivo.[21,22] Histological change of the normal organs was investigated to determine the tolerable safety profile. No distinct changes in the fundamental structure of normal organs (heart, liver, spleen, lung, and kidney) were observed, indicating a tolerable safety profile of the treatment (Figure 5C).

Encouraged by the excellent tumor-targeting ability of [89]Zr@CS-GA-MLPs, we further investigated the anti-tumor activity of [89]Zr@CS-GA-MLPs. GA, which is the main
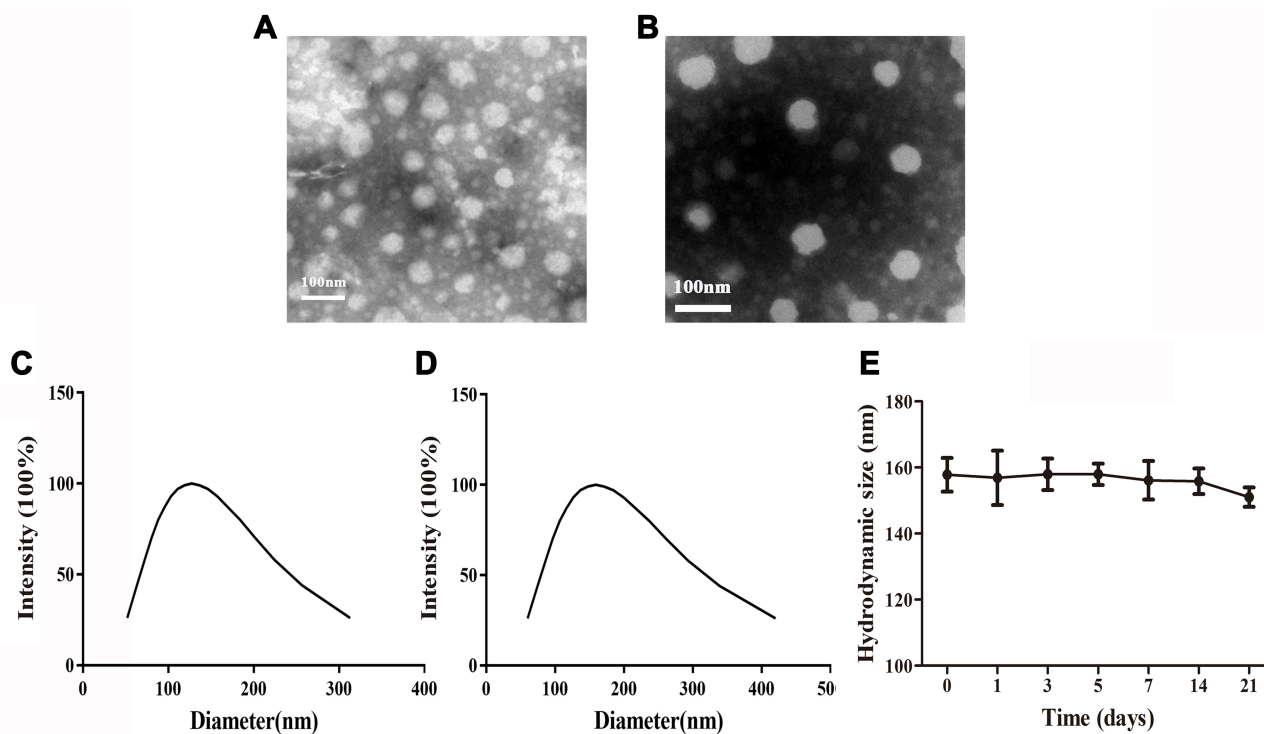

Figure 4 Characterization of CS-MLPs. (**A**) Morphology of blank liposomes. (**B**) Morphology of CS-MLPs. (**C**) Hydrodynamic size of blank liposomes. (**D**) Hydrodynamic size of CS-MLPs. (**E**) Stability of CS-MLPs in storage at 4°C for 3 weeks.
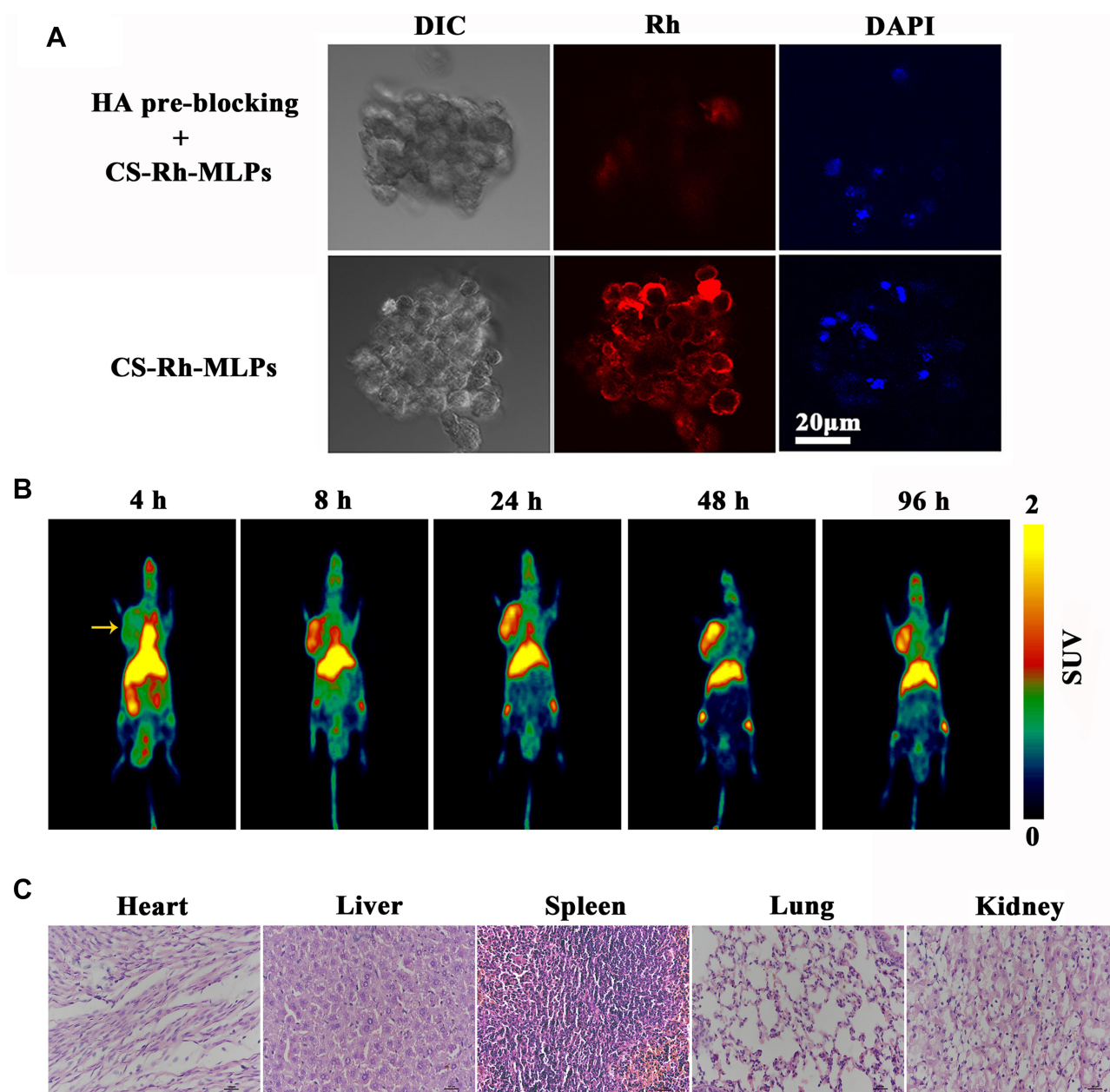**Abbreviations:** CS, chitosan; MLP, multifunctional liposome.

Figure 5 Uptake of CS-MLPs by CD44 overexpressing cells and distribution in vivo. (**A**) Fluorescence images of the pre-blocking and target groups. (**B**) Micro PET images of nude mice bearing subcutaneously implanted human xenografts of MDA-MB-231 cells at 4, 8, 24, 48, and 96 h. Images show high levels of [89]Zr-labeled CS-MLPs accumulation in the tumor (left side of axillary). Yellow arrows indicate the tumor. (**C**) Histological images of heart, liver, spleen, lung, and kidney.
Abbreviations: CS, chitosan; MLP, multifunctional liposome; CD, cluster of differentiation; PET, positron emission tomography; [89]Zr, zirconium-89; HA, hyaluronic acid; Rh, rhodamine B; DAPI, 4',6-diamidino-2-phenylindole; DIC, differential interference contrast; SUV, standard uptake value

active ingredient of gamboge resin secreted from the plant Garcinia hanburyi, shows inherent anti-tumor activity and has huge potential for the prevention and treatment of cancer. However, the effect of GA is limited due to its poor solubility and dose-limited by its liver and kidney toxicity.[23] Here, GA was loaded into MLPs to determine the therapeutic efficacy of [89]Zr-labeled chitosan-modified liposomes. The anti-tumor efficacy of GA-loaded non-target MLPs and GA-loaded

target MLPs were investigated. Mice bearing MDA-MB-231 tumors were injected intravenously with non-target MLPs and target MLPs (GA, 2mg/kg). As shown in Figure 6A, no distinct changes in body weight were observed in the target group, indicating a tolerable safety profile of the treatment (Figure 6A). After 28 days of treatment, the target group showed remarkable tumor inhibition compared with the non-target group and control group (p < 0.05)

Table 2 Accumulation of Radioactivity (%ID/g) in ROI in the Tissues of Mice at Different Time Points (n = 3, Mean ± SD)

Time (h)	Tumor	Heart	Spleen	Kidney	Lung	Liver
2	3.46±0.33	10.40±0.96	8.13±0.22	7.33±1.05	4.25±1.03	17.61±1.45
6	4.13±0.24	12.27±1.01	10.69±1.22	6.43±2.14	3.83±0.83	16.12±1.24
24	6.61±0.30*	6.85±0.39	5.82±2.08	5.64±1.62	3.29±0.90	13.30±1.15
48	7.52±0.43	6.13±0.29	6.47±0.86	4.16±1.34	3.38±2.43	12.31±1.02
96	7.04±1.00	5.37±0.48	4.7±1.23	2.57±1.16	1.69±0.58	10.90±2.39

Notes: *Compared with the accumulation of radioactivity in ROI at 4 h, $p<0.05$.
Abbreviations: ID/g, injected dose per gram of tissue; ROI, regions of interest.

(Figure 6B). A distinct change in the fundamental structure of tumor tissue was observed in the target group. As shown in Figure 6C, HE staining revealed obvious necrosis and hemorrhage in the tissues of the target group. These findings suggest remarkable anti-tumor efficacy of the target group in vivo, probably due to the excellent tumor-targeting ability and killing of CD44^{+} CSCs. Taken together, these data suggest that [89]Zr@CS-MLPs are an excellent drug carrier for PET-guided, CD44-targeted TNBC therapy in the future.

CD44 is an important cell-adhesion molecule required for tumor progression and metastasis.[24] It can bind to the extracellular matrix component, HA and leads to tumorigenesis. For this reason, HA-decorated nanocarriers have undergone extensive research for active targeting against CD44^{+}
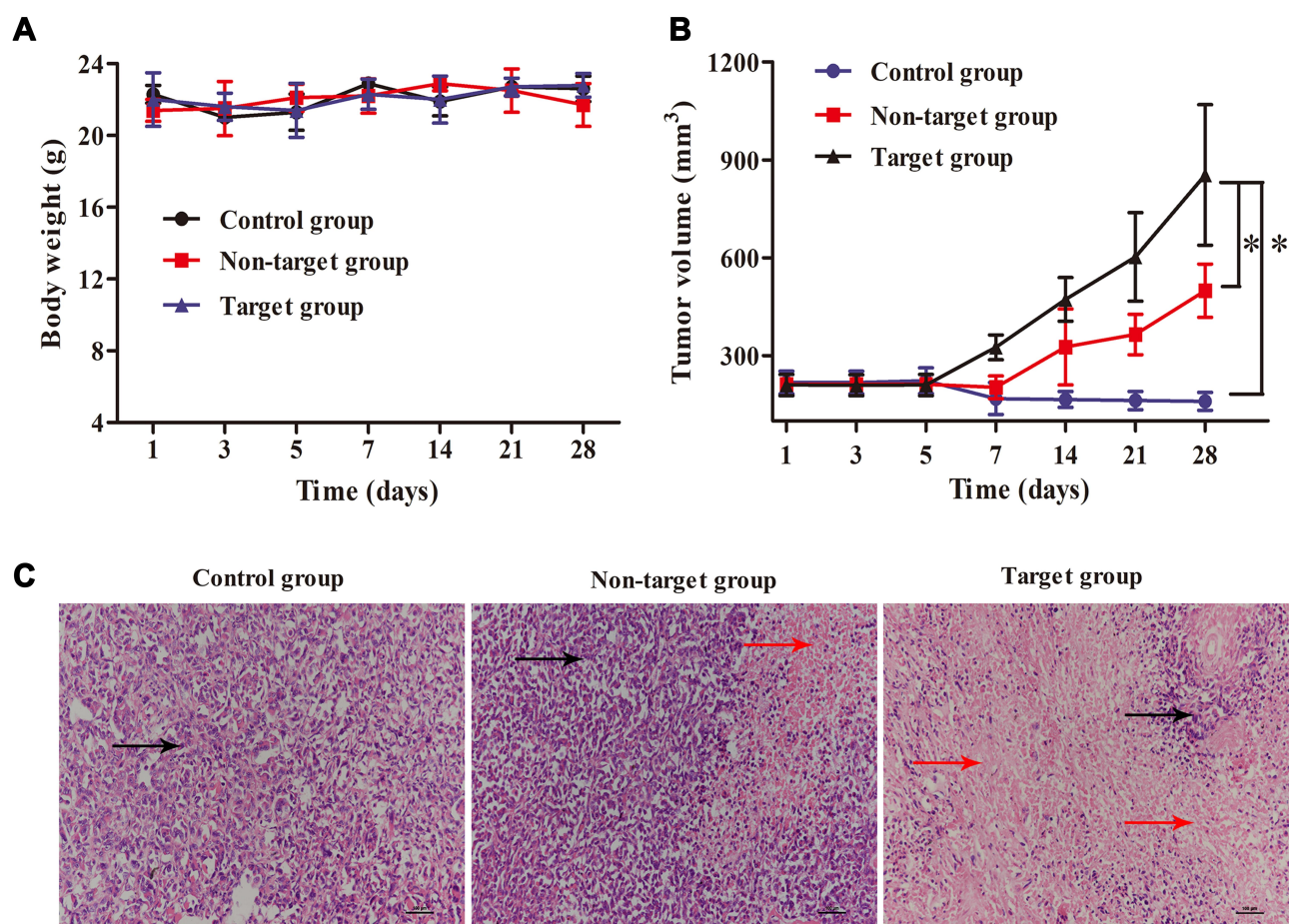

Figure 6 Anti-tumor activity of [89]Zr@CS-GA-MLPs in vivo. (**A**) Body weight of control group, non-target group, and target group during 28 days of treatment. (**B**) Tumor volume of control group, non-target group, and target group during 28 days of treatment (* $p<0.05$). (**C**) Histological images of tumors of control group, non-target group, and target group after 28 days of treatment. Black arrows indicate the tumor tissues, and red arrows indicate the necrosis tissues.
Abbreviations: CS, chitosan; MLP, multifunctional liposome; [89]Zr, zirconium-89.

CSCs.[25] CS is a natural linear aminopolysaccharide and its chemical structure is partially similar to HA. The high reactivity of functional groups in CS makes it easy to be chemically modified. In this study, CS-MLPs carrying ^{89}Zr on the surface were conjugated with DFO via the amine groups of CS. Furthermore, a previous study showed that CS-based nanoparticles could specifically target CD44-overexpressed cancer stem-like cells but not CD44 expressed on normal stem cells.[11] Thus, ^{89}Zr-labeled CS-decorated MLPs were prepared in the present study to provide sensitive target visualization. ^{89}Zr is a radionuclide with a long half-life and produces positrons useful for high-resolution PET imaging.[26] We found that ^{89}Zr@CS-MLPs had higher values in the tumor and could show real-time behavior quantitatively in vivo. When loaded with the anti-tumor drug, GA, the MLPs demonstrated enhanced anti-tumor efficacy in vivo. Hence, ^{89}Zr@CS-MLPs constitute a promising potential drug carrier for TNBC-targeted therapy. It is emphasized that the targeted therapy of CSCs does not reject the treatment for proliferating tumor cells. Differentiated and proliferated normal tumor cells are the main components of tumors, and the cytokines produced by them have a significant effect on the body's cachexia state and tumor immune escape.[27,28] Hence, killing CD44$^+$ normal tumor cells is also important for the tumor therapy. In this study, although chitosan-modified liposome may not only target CSCs rather than bulk cancer cells, CD44-target MLPs could effectively inhibit tumor growth compared with non-target group. Further work is needed to explore the anti-tumor mechanism of the multifunctional targeted liposomes and identify additional appropriate drugs that kill TNBC CSCs. Since the tumor microenvironment is hypoxic, compared with normal tissues due to imperfect vascular networks,[29] our future work will focus mainly on cytotoxic anti-cancer agents that are responsive to hypoxia.

Conclusion

In this study, we demonstrated the biological and molecular basis of CS targeting CD44 and showed that breast CSC marker CD44 is overexpressed on 3D mammospheres and TNBC tissues. For the first time, we used molecular docking and dynamics methods to gain detailed insights into the binding process and mechanisms between CD44 and CS. We constructed a novel CS-decorated MLP to target CD44$^+$ TNBC CSCs in vitro and in vivo. Rh was loaded in the CS-MLPs, and a confocal laser experiment indicated that CS-MLPs can bind to CD44-overexpressed 3D mammospheres. ^{89}Zr was used to label the CS-

decorated MLPs and to trace accurately and quantitatively the nanocarriers in vivo, in real-time. ^{89}Zr@CS-MLPs showed enhanced and persistent accumulation in TNBC cell line MDA-MB-231 tumors. In addition, when loaded with GA, ^{89}Zr@CS-MLPs showed excellent tumor-targeting ability compared with the non-target group, suggesting that ^{89}Zr@CS-MLPs may be an excellent drug carrier for PET-image-guided, CD44-targeted TNBC therapy in the future.

Funding

Disclosure

The authors report no conflicts of interest in this work.

References

1. Cardoso F, Spence D, Mertz S, et al. Global analysis of advanced/metastatic breast cancer: decade report (2005–2015). *Breast*. 2018;39:131–138. doi:10.1016/j.breast.2018.03.002
2. Shah TA, Guraya SS. Breast cancer screening programs: review of merits, demerits, and recent recommendations practiced across the world. *J Microscopy Ultrastructure*. 2017;5(2):59–69. doi:10.1016/j.jmau.2016.10.002
3. Bianchini G, Balko JM, Mayer IA, Sanders ME, Gianni L. Triple-negative breast cancer: challenges and opportunities of a heterogeneous disease. *Nat Rev Clin Oncol*. 2016;13(11):674–690. doi:10.1038/nrclinonc.2016.66
4. Batlle E, Clevers H. Cancer stem cells revisited. *Nat Med*. 2017;23 (10):1124–1134. doi:10.1038/nm.4409
5. Dawood S, Austin L, Cristofanilli M. Cancer stem cells: implications for cancer therapy. *Oncology*. 2014;28(12):1101–1107, 1110.
6. Al-Hajj M, Wicha MS, Benito-Hernandez A, Morrison SJ, Clarke MF. Prospective identification of tumorigenic breast cancer cells. *Proc Natl Acad Sci U S A*. 2003;100(7):3983–3988. doi:10.1073/pnas.0530291100
7. Zheng Z, Shao N, Weng H, et al. Correlation between epidermal growth factor receptor and tumor stem cell markers CD44/CD24 and their relationship with prognosis in breast invasive ductal carcinoma. *Medical Oncol*. 2015;32(1):275. doi:10.1007/s12032-014-0275-2
8. Wang H, Wang L, Song Y, et al. CD44(+)/CD24(-) phenotype predicts a poor prognosis in triple-negative breast cancer. *Oncol Lett*. 2017;14 (5):5890–5898.

9. Pandey S, Mahtab A, Rai N, Rawat P, Ahmad FJ, Talegaonkar S. Emerging role of CD44 receptor as a potential target in disease diagnosis: a patent review. *Recent Pat Inflamm Allergy Drug Discov.* 2017;11(2):77–91. doi:10.2174/1872213X11666170907111858

10. Morath I, Hartmann TN, Orian-Rousseau V. CD44: more than a mere stem cell marker. *Int J Biochem Cell Biol.* 2016;81(Pt A):166–173. doi:10.1016/j.biocel.2016.09.009

11. Rao W, Wang H, Han J, et al. Chitosan-decorated doxorubicin-encapsulated nanoparticle targets and eliminates tumor reinitiating cancer stem-like cells. *ACS Nano.* 2015;9(6):5725–5740.

12. Zhang X, Li F, Zheng Y, et al. Propofol reduced mammosphere formation of breast cancer stem cells via PD-L1/Nanog in vitro. *Oxid Med Cell Longev.* 2019;2019:9078209.

13. Cioce M, Gherardi S, Viglietto G, et al. Mammosphere-forming cells from breast cancer cell lines as a tool for the identification of CSC-like- and early progenitor-targeting drugs. *Cell Cycle.* 2010;9 (14):2878–2887. doi:10.4161/cc.9.14.12371

14. Moore-Smith L, Forero-Torres A, Stringer-Reasor E. Future developments in neoadjuvant therapy for triple-negative breast cancer. *Surg Clin North Am.* 2018;98(4):773–785. doi:10.1016/j.suc.2018.04.004

15. Diaz Casas S, Lancheros Garcia E, Sanchez Campo A, et al. Clinical behavior of triple negative breast cancer in a cohort of latin american women. *Cureus.* 2019;11(6):e4963.

16. Gao J, Li W, Guo Y, Feng SS. Nanomedicine strategies for sustained, controlled and targeted treatment of cancer stem cells. *Nanomedicine.* 2016;11(24):3261–3282. doi:10.2217/nnm-2016-0261

17. Zhao D, Yu S, Sun B, Gao S, Guo S, Zhao K. Biomedical applications of chitosan and its derivative nanoparticles. *Polymers.* 2018;10:4. doi:10.3390/polym10040462

18. Kim UJ, Lee YR, Kang TH, Choi JW, Kimura S, Wada M. Protein adsorption of dialdehyde cellulose-crosslinked chitosan with high amino group contents. *Carbohydr Polym.* 2017;163:34–42. doi:10.1016/j.carbpol.2017.01.052

19. Fenaroli F, Repnik U, Xu Y, et al. Enhanced permeability and retention-like extravasation of nanoparticles from the vasculature into tuberculosis granulomas in zebrafish and mouse models. *ACS Nano.* 2018;12(8):8646–8661. doi:10.1021/acsnano.8b04433

20. Muppidi K, Pumerantz AS, Wang J, Betageri G. Development and stability studies of novel liposomal vancomycin formulations. *ISRN Pharm.* 2012;2012:636743. doi:10.5402/2012/636743

21. Yu B, Goel S, Ni D, et al. Reassembly of [89]Zr-labeled cancer cell membranes into multicompartment membrane-derived liposomes for pet-trackable tumor-targeted theranostics. *Adv Mater.* 2018;30(13): e1704934. doi:10.1002/adma.201704934

22. Samuelsson E, Shen H, Blanco E, Ferrari M, Wolfram J. Contribution of Kupffer cells to liposome accumulation in the liver. *Colloids Surf B Biointerfaces.* 2017;158:356–362. doi:10.1016/j.colsurfb.2017.07.014

23. Wang X, Chen W. Gambogic acid is a novel anti-cancer agent that inhibits cell proliferation, angiogenesis and metastasis. *Anticancer Agents Med Chem.* 2012;12(8):994–1000. doi:10.2174/187152012802650066

24. Chen C, Zhao S, Karnad A, Freeman JW. The biology and role of CD44 in cancer progression: therapeutic implications. *J Hematol Oncol.* 2018;11(1):64. doi:10.1186/s13045-018-0605-5

25. Wickens JM, Alsaab HO, Kesharwani P, et al. Recent advances in hyaluronic acid-decorated nanocarriers for targeted cancer therapy. *Drug Discov Today.* 2017;22(4):665–680. doi:10.1016/j.drudis.2016.12.009

26. Fischer G, Seibold U, Schirrmacher R, Wangler B, Wangler C. (89) Zr, a radiometal nuclide with high potential for molecular imaging with PET: chemistry, applications and remaining challenges. *Molecules.* 2013;18(6):6469–6490. doi:10.3390/molecules18066469

27. Patel HJ, Patel BM. TNF-α and cancer cachexia: molecular insights and clinical implications. *Life Sci.* 2017;170:56–63. doi:10.1016/j.lfs.2016.11.033

28. Liu Y, Cao X. Immunosuppressive cells in tumor immune escape and metastasis. *J Molecular Med.* 2016;94(5):509–522. doi:10.1007/s00109-015-1376-x

29. Graham K, Unger E. Overcoming tumor hypoxia as a barrier to radiotherapy, chemotherapy and immunotherapy in cancer treatment. *Int J Nanomedicine.* 2018;13:6049–6058. doi:10.2147/IJN.S140462